

Research article

Jun Gou, Hilal Cansizoglu, Cesar Bartolo-Perez, Soroush Ghandiparsi, Ahmed S. Mayet, Hossein Rabiee-Golgir, Yang Gao, Jun Wang, Toshishige Yamada, Ekaterina Ponizovskaya Devine, Aly F. Elrefaie, Shih-Yuan Wang and M. Saif Islam*

Rigorous coupled-wave analysis of absorption enhancement in vertically illuminated silicon photodiodes with photon-trapping hole arrays

<https://doi.org/10.1515/nanoph-2019-0164>

Received June 5, 2019; revised August 7, 2019; accepted August 26, 2019

Abstract: In this paper, we present a rigorous coupled-wave analysis (RCWA) of absorption enhancement in all-silicon (Si) photodiodes with integrated hole arrays of different shapes and dimensions. The RCWA method is used to analyze the light propagation and trapping in the photodiodes on both Si-on-insulator (SOI) and bulk Si substrates for the datacom wavelength at about 850 nm. Our calculation and measurement results show that funnel-shaped holes with tapered sidewalls lead to low back-reflection. A beam of light undergoes a deflection subsequent to the diffraction in the hole array and

generates laterally propagating waves. SOI substrates with oxide layers play an important role in reducing the transmission loss, especially for deflected light with higher-order diffraction from the hole array. Owing to laterally propagating modes and back-reflection on the SiO₂ film, light is more confined in the thin Si layer on the SOI substrates compared to that on the bulk Si substrates. Experimental results based on fabricated devices support the predictions of the RCWA. Devices are designed with a 2- μm -thick intrinsic layer, which ensures ultrafast impulse response (full-width at half-maximum) of 30 ps. Measurements for integrated photodiodes with funnel-shaped holes indicate an enhanced external quantum efficiency of more than 55% on the SOI substrates. This represents more than 500% improvement compared to photodiodes without integrated phototrapping nanoholes.

*Corresponding author: **M. Saif Islam**, Electrical and Computer Engineering, University of California – Davis, Davis, CA 95618, USA, e-mail: sislam@ucdavis.edu

Jun Gou: Electrical and Computer Engineering, University of California – Davis, Davis, CA 95618, USA; and State Key Laboratory of Electronic Thin Films and Integrated Devices, University of Electronic Science and Technology of China, Chengdu 610054, China. <https://orcid.org/0000-0002-8017-9287>

Hilal Cansizoglu, Cesar Bartolo-Perez, Soroush Ghandiparsi, Ahmed S. Mayet, Hossein Rabiee-Golgir and Yang Gao: Electrical and Computer Engineering, University of California – Davis, Davis, CA 95618, USA

Jun Wang: State Key Laboratory of Electronic Thin Films and Integrated Devices, University of Electronic Science and Technology of China, Chengdu 610054, China

Toshishige Yamada: W&WSens Devices, Inc., 4546 El Camino, Suite 215, Los Altos, CA 94022, USA; and Electrical Engineering, Baskin School of Engineering, University of California – Santa Cruz, Santa Cruz, CA 95064, USA

Ekaterina Ponizovskaya Devine and Shih-Yuan Wang: W&WSens Devices, Inc., 4546 El Camino, Suite 215, Los Altos, CA 94022, USA

Aly F. Elrefaie: Electrical and Computer Engineering, University of California – Davis, Davis, CA 95618, USA; and W&WSens Devices, Inc., 4546 El Camino, Suite 215, Los Altos, CA 94022, USA

Keywords: all-silicon photodiode; nanoholes; phototrapping; rigorous coupled-wave analysis.

1 Introduction

For the widely used short-reach (<300 m) multimode data communication wavelength of 840–860 nm, low-cost monolithically integrated photodiodes on silicon (Si) with high efficiency and high speed are highly desirable to address the data traffic bottleneck in data centers [1]. An all-Si PIN photodiode offers clear advantages of IC process compatibility to significantly reduce the cost in manufacturing and packaging [2]. However, it is difficult for a traditional Si photodiode used predominantly in the visible wavelength regime to meet the requirements on both high efficiency and high speed at near-infrared wavelengths. At the wavelength of 850 nm, the intrinsic layer in an Si photodiode with a low absorption coefficient (535 cm⁻¹) would need a thickness of more than 13 μm to achieve an external

quantum efficiency (EQE) of more than 50% [3]. Such thickness leads to a long transit time of photogenerated carriers and limits the data rate to a maximum of 4 Gb/s. Therefore, the absorption of the intrinsic layer needs to be effectively enhanced without increasing the thickness.

Microscale and nanoscale structures with a characteristic size comparable to or smaller than the wavelength on semiconductor surfaces have been proposed to manipulate light due to distinctly different optical and thermal properties compared to flat surfaces. The abnormal radiation phenomenon of the incident electromagnetic wave, including surface plasmon polaritons [4–6], Wood's anomaly [7], and cavity resonance [8–10], can be induced mainly due to multiple reflection and diffraction effects of the structures. Several types of microscale and nanoscale structures have been demonstrated in the absorption enhancement of energy conversion systems, such as solar cells [11, 12] and thermophotovoltaic devices [13], including nanowires [10, 11, 14, 15], nanorods [16], nanodisks [17], nanocones [18], nanopyramids [19, 20], nanoholes [21, 22], and other grating structures [23–26]. Our recent experimental studies [27, 28] showed that an array of nanoholes integrated on a 2- μm -thick Si film effectively traps light with wavelengths between 800 and 950 nm and can be used to achieve a high EQE (40–60%) in Si photodetectors while ensuring ultrafast impulse response (full-width at half-maximum) of 30 ps. High-speed Ge-on-Si photodiodes with photon-trapping holes have also been demonstrated with improved EQE at wavelengths between 1200 and 1800 nm [29]. Light-trapping properties of such hole arrays in Si were investigated by finite-difference time-domain method [27] and the effects of hole shape and tapering angle of funnel-shaped holes on the EQE of the photodiodes were analyzed and discussed in detail [27, 28]. However, there are still questions that need to be answered: How does the substrate influence the light-trapping properties of the holes, what fraction of light is laterally guided, and where is the guided light mostly confined?

In this work, to understand the underlying physical principle of the light-trapping effect of hole arrays integrated in the photodiodes, the rigorous coupled-wave analysis (RCWA) method, which can provide more details on light propagation and the interaction between light and materials, was employed [30–33]. We apply the RCWA method to calculate the reflection and transmission efficiencies of diffraction orders in Si with hole arrays on both bulk Si and Si-on-insulator (SOI) substrates. The deflection of light with nonzero diffraction orders guides the vertical incident light in laterally propagating modes. Back-reflection of buried oxide (BOX) layers on SOI substrates

are calculated for the light with different orders and deflection angles. RCWA provides theoretical explanations for light trapping and absorption enhancement in hole-based Si photodiodes designed on SOI substrates. Our calculations and experimental results demonstrate that light is most effectively trapped in photodiodes integrated with funnel-shaped holes on the SOI wafers with significantly reduced reflection and transmission loss compared to photodiodes with cylindrical holes or on bulk Si substrates. Si PIN photodiodes with hole arrays in hexagonal lattice are fabricated on both bulk Si and SOI wafers. Using both theoretical and experimental approaches, we investigated the effects of hole shape, presence of substrates, hole diameter and period on light trapping, and degree of absorption enhancement in the photodiodes at the datacom wavelengths at about 850 nm. With a 2- μm -thick *i*-Si layer, EQE of photodiodes with integrated funnel-shaped holes are 20%–25% on the bulk Si substrate. This can be enhanced to 55% when the device is fabricated on an SOI wafer. Given that a photodiode without integrated holes on bulk Si substrates exhibits ~10% EQE, this represents more than 500% improvement over an Si PIN photodiode in the absence of photon-trapping hole structures.

2 Design and calculation

The photodiodes with photon-trapping holes have an NIP mesa structure as shown in Figure 1A and B. SOI wafer (Figure 1A) and bulk Si wafer (Figure 1B) are used as the substrates. A 2- μm -thick *i*-Si film acts as the absorption region with 0.2 μm P-doped n^+ thin layer as the top *n*-ohmic contact and 0.2 μm $p^{++}\text{-Si}_{0.988}\text{Ge}_{0.01}\text{B}_{0.002}$ film as the bottom *p*-contact layer. Microscale and nanoscale holes that span the *n*, *i*, and *p* layers are integrated in the active region. Figure 1C shows the active region of an Si PIN photodiode (30 μm diameter) with integrated submicron holes. The thinner ring and the thicker opened ring are *n*-ohmic metal on *n*-mesa and *p*-ohmic metal on *p*-mesa, respectively. The detailed fabrication process and EQE characteristics of the photodiodes were reported in our previous studies [27, 28]. Photodiodes with hole arrays arranged in hexagonal lattice, as shown in Figure 1D, were fabricated on both bulk Si and SOI wafers with hole diameters ranging from 630 to 1300 nm and periods from 900 to 1700 nm. Holes were etched as gradual funnel shapes with tapered sidewalls (~65°). For the purpose of comparison, photodiodes with cylindrical hole arrays in hexagonal lattice with a hole diameter of 700 nm and a period of 1000 nm were also fabricated on bulk Si and SOI wafers.

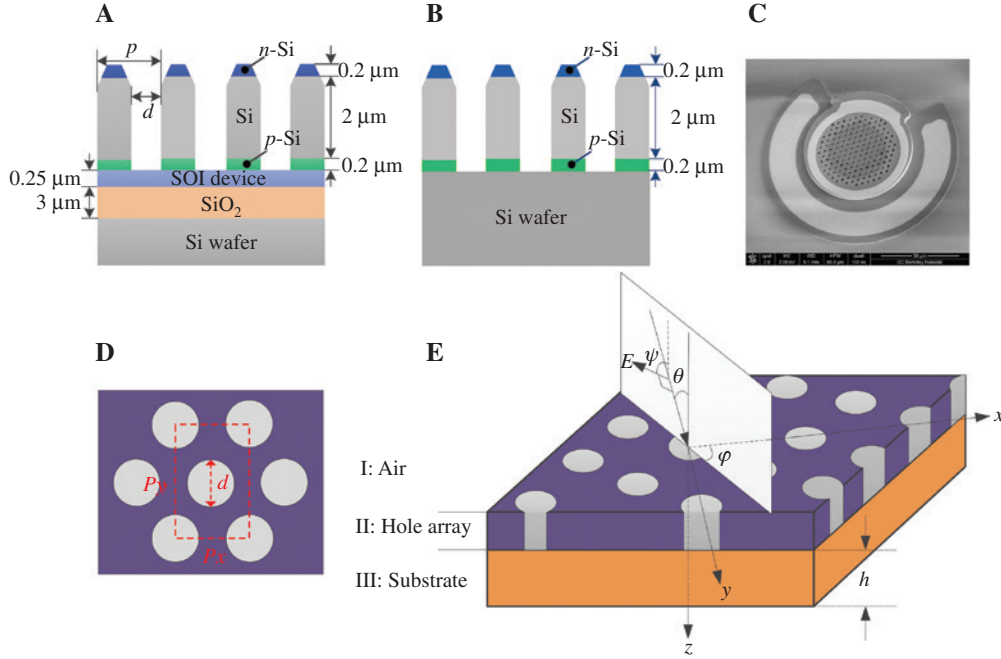


Figure 1: Design of photodiodes with integrated photon-trapping holes on both SOI and bulk Si wafers.

(A and B) The n - i - p photodiode structure on an SOI wafer (A) and a bulk Si wafer (B), showing the integrated funnel-shaped holes that span the n , i , and p layers. (C) Scanning electron micrograph of the active region of an Si PIN photodiode (30 μm diameter). (D) Holes in hexagonal lattice. (E) Periodic hole array illuminated by a plane wave with a rectangular Cartesian coordinate system added for clarity.

Absorption in photodiodes with photon-trapping holes with different diameters and periods were calculated by applying the RCWA method. RCWA is a rigorous grating diffraction theory that is suited to study the mechanism of the diffraction of light from periodically structured surfaces. In RCWA, the devices and electromagnetic fields are represented by a sum of spatial harmonics, as Maxwell's equations are solved in Fourier space. The eigenmodes of electric and magnetic fields in the grating layer are calculated and analytically propagated. The problem is then solved by matching boundary conditions at each interface using scattering matrices. The hole-integrated i -Si layers in our photodiodes were treated as crossed gratings (or 2D gratings), which are periodic in the x and y directions with periods of p_x and $p_y = \sqrt{3}p_x$, respectively [34]. Figure 1E shows a schematic representation of a crossed grating with hole array in hexagonal lattice. In the attached rectangular Cartesian coordinate system, the x and y axes are parallel to periodic directions and the z axis is perpendicular to the grating plane. The device is divided into three layers along the z direction: the incident layer (I: air, $z < 0$), the grating layer (II: Si with hole array, $0 \leq z \leq h$), and the substrate layer [III: Si for bulk wafer or Si on silicon oxide (SiO_2) film for the SOI wafer, $z > h$]. The incident layer and the substrate layer are homogeneous media with permittivities of ϵ_{air} and ϵ_{Si} , respectively. For the sake

of simplicity, holes in the grating layer are considered as cylindrical in shape. The grating layer has a thickness of 2 μm , and its permittivity, $\epsilon(x, y)$, is a piecewise-constant function taking two values, ϵ_{Si} and ϵ_{air} . ϵ_{Si} is taken to be a complex quantity to accommodate lossy grating,

$$\epsilon_{\text{Si}} = \epsilon' - i\epsilon'' = n_{\text{Si}}^2 \quad (1)$$

The electric field E causes the polarization of atoms in Si to create electric dipole moments that augment the total displacement flux (D) with an electric susceptibility of χ_e ,

$$D = \epsilon_0 E + \epsilon_0 \chi_e E \quad (2)$$

where ϵ_0 is the permittivity of free space. A complex electric susceptibility leads to a complex permittivity of Si ($\epsilon_{\text{Si}} = \epsilon_0 + \epsilon_0 \chi_e$). The imaginary part of complex permittivity (ϵ'') accounts for loss (light absorption) in Si due to damping of the vibrating dipole moments. The loss in Si may also be considered as an equivalent conductor loss. A conduction current density (J) will exist,

$$J = i\omega(\epsilon' - i\epsilon'')E = \omega\epsilon''E + i\omega\epsilon'E \quad (3)$$

where ω is the frequency of the electric field. $\omega\epsilon''$ can be considered as an effective conductivity that is related to Joule heating. The refractive index of the incident layer

and the cylindrical holes in the grating is $n_{\text{air}} = 1$, whereas the refractive index of the Si substrate and the surrounding Si layer in the grating is $n_{\text{Si}} = 3.65 - 0.04i$ at the wavelength of 850 nm [3]. The propagation direction of the incident plane wave is given by polar angle θ , azimuthal angle φ , and polarization angle ψ , as indicated in Figure 1E.

The formulation of RCWA is presented in Section S1 in Supplementary Material. The calculations were carried out by Matlab programs with the algorithm based on Ref. [34]. As our photodiodes are nearly perpendicularly illuminated by a monochromatic electromagnetic plane wave, we used $\theta = 0^\circ$, $\varphi = 0^\circ$, and $\psi = 90^\circ$ (TE polarization) in the calculations. In this case, the electromagnetic field vectors in all regions have only the components along the y direction for the electric fields and nonzero components along the x and z directions for the magnetic fields.

3 Results and discussion

3.1 Lower reflection of funnel-shaped hole array with shorter hole-hole distance

According to the grating theory, the diffraction order $[m, n]$ of reflected waves from a vertically illuminated crossed grating is limited by the ratio between the period (p) of hole array and the wavelength (λ) of incident light [35]:

$$|m|, |n| < \frac{p}{\lambda} \quad (4)$$

In our design, the periods of hole arrays integrated in the photodiodes are distributed in the range of $\lambda < p \leq 2\lambda$

in the x direction, so only reflected waves in the 0th and ± 1 st orders exist. However, holes are arranged in 2D hexagonal lattice with inconsistent periods in the x and y directions ($p_y = \sqrt{3}p_x$), so ± 2 nd-order diffractions should also be considered. Therefore, the total reflection (R_{total}) of the hole-based i -Si layer can be calculated by $R_{\text{total}} = \sum_{m,n} \eta_{Rmn}$, $m, n = 0, \pm 1, \pm 2$.

The RCWA calculated reflection diffraction efficiencies (R_N) of the hole-based i -Si layers with different periods at orders from $N=0$ to $N=3$ are shown in Figure 2A for an Si substrate (assumed to have an infinite thickness for the RCWA model used). Period (p) in all the figures in this paper means the period in the x direction (p_x). $R_{N=0}$ is the reflection diffraction efficiency at the 0th order ($[0\ 0]$), whereas $R_{N=1}$ includes all the reflection diffraction efficiencies (η_{Rmn}) at the ± 1 st order with one of m and n equal to ± 1 and the other one lower than or equal to ± 1 , including $[0\ 1]$, $[0\ -1]$, $[-1\ 0]$, $[-1\ 1]$, $[-1\ -1]$, $[1\ -1]$, $[1\ 0]$, and $[1\ 1]$. $R_{N=2}$ and $R_{N=3}$ are calculated in a similar way that has more diffraction orders. $R_{N=0}$ has the highest diffraction efficiency compared to higher orders. $R_{N=3=0}$ demonstrates that the highest diffraction order is limited to $N=2$ ($m, N=\pm 2$). It is shown that the reflection is higher at larger periods for the 0th-order reflected wave ($R_{N=0}$) and relatively lower at larger periods for $R_{N=1}$ and $R_{N=2}$. However, the total reflection of hole-integrated i -Si layer generally increases with the increase of period as $R_{N=0}$ makes a major contribution. When the diameter of holes is constant, a smaller period means a higher fill ratio of photon-trapping holes in Si, whereas a larger period provides more area of flat Si film with higher surface reflection.

The measured reflection of photodiodes with funnel-shaped holes in hexagonal lattice with different periods

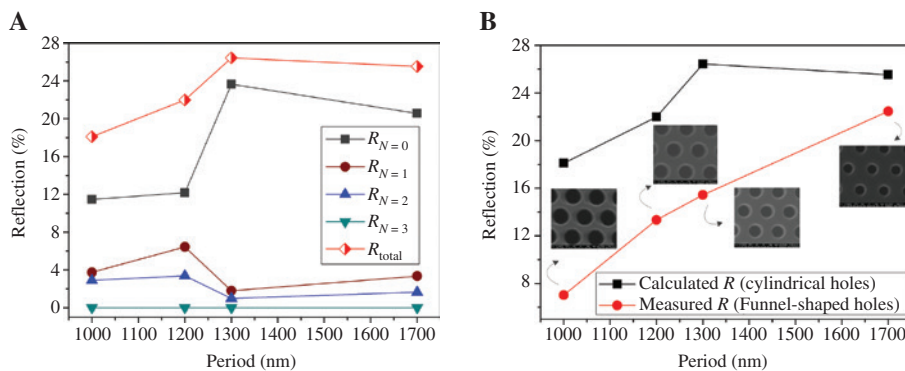


Figure 2: Calculated and measured reflection properties of photon-trapping holes.

(A) RCWA calculated reflection diffraction efficiency (R_N) at different diffraction orders (N) and total reflection (R_{total}) versus period (in the x direction) for cylindrical hole array in hexagonal lattice with a diameter of 700 nm on Si substrate. (B) RCWA calculated reflection of cylindrical hole array and measured reflection of funnel-shaped hole array in hexagonal lattice at different periods (in the x direction) with a diameter of 700 nm. (Inset) Top views of funnel-shaped hole arrays in hexagonal lattice integrated in the photodiodes with different periods. Note that the calculation is for cylindrical holes and the measured data are for funnel-shaped holes.

on bulk Si wafer are shown and compared to the RCWA calculated reflection of cylindrical hole-based *i*-Si layer on the bulk Si substrate in Figure 2B. The measured reflection of photodiodes are much lower than the calculated values. Funnel-shaped holes provide a gradually changing effective refractive index compared to cylindrical holes and create an effect similar to a graded refractive index antireflection coating [36]. The decrease of reflection is more significant for smaller periods (>50% reduction of the reflection when $p=1000/1200/1300$ nm) as most of the top Si surface is etched into tapered sidewalls. Top views of funnel-shaped holes with a diameter of 700 nm and different periods are shown in Figure 2B (inset). The diameter of a funnel hole refers to the diameter of the cylindrical part at the bottom of the holes. The tapered sidewalls of funnel-shaped holes were formed by lateral etch using reactive ion etching, which expanded the designed hole diameter at the opening of the holes on the device surface. At higher period ($p=1700$ nm), additional flat Si surface with higher reflection was retained due to the large spacing between adjacent holes.

3.2 Lower transmission due to laterally propagating waves and back-reflection

The diffraction order $[m, n]$ of transmitted waves in the device layer of SOI (p -Si) from a vertically illuminated crossed grating is limited by

$$|m|, |n| < \frac{pn_s}{\lambda} \quad (5)$$

n_s is the refractive index of the substrate ($n_s = 3.65 - 0.04i$). The highest diffraction order of transmitted waves from

the hole-based *i*-Si layer with a period of $\lambda < p \leq 2\lambda$ in the x direction to the SOI device layer should be $N=7$ ($m, n = \pm 7$), and more diffraction orders should be considered in the y direction ($p_y = \sqrt{3}p_x$). The RCWA calculated transmission diffraction efficiencies (T_N) of cylindrical hole-based *i*-Si layers with different periods on an Si substrate (assumed to have an infinite thickness for the RCWA model used) at diffraction orders from $N=0$ to $N=5$ are shown in Figure 3A. Similar to the calculation of R_N , T_N includes all the transmitted waves (η_{Tmn}) with one of m and n equal to $\pm N$ and the other one lower than or equal to $\pm N$. Generally, $T_{N=0}$ (η_{T00}) has the highest transmission diffraction efficiency. However, relatively high diffraction efficiency for $T_{N=1}$ can be observed especially at smaller period ($p=1000$ nm). High total transmission of about 65%–70% are observed as the period varies. The absorption of the hole-based *i*-Si layer can be calculated by $A = 1 - R_{\text{total}} - T_{\text{total}}$ for a photodiode on Si substrate. However, our photodiode structure was grown on an SOI substrate with a 0.25 μm device layer over a 3 μm BOX layer. The SiO_2 layer acting as a back-reflection layer creates multiple reflection and diffraction effects for the transmitted waves and leads to enhanced absorption and EQE performance of the photodiodes.

Although the light is perpendicularly incident to the hole-based photodiodes, the reflected and transmitted waves undergo a deflection subsequent to the diffraction in the hole array. The deflection angle (θ_N) of N th-order transmitted wave (T_N) in the device layer of SOI can be calculated by Eq. (6) for different periods (p), and the results are shown in Table 1. It should be noted that our photodiodes have 2D periodic holes in hexagonal lattice with inconsistent periods in the x and y directions ($p_y = \sqrt{3}p_x$),

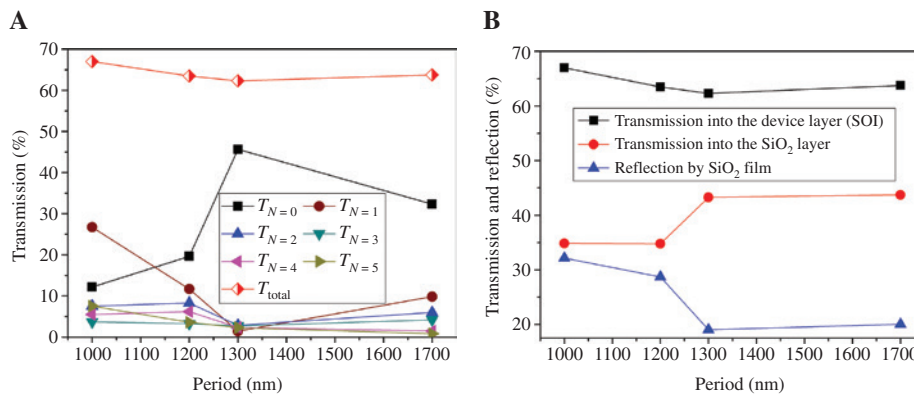


Figure 3: Calculated transmission properties of photon-trapping holes and back reflection by SiO_2 film.

(A) RCWA calculated total transmission (T_{total}) and transmission diffraction efficiency (T_N) from hole-based *i*-Si layer to the SOI device layer with the order from $N=0$ to $N=5$ versus period (in the x direction) for hexagonal hole array with a diameter of 700 nm on Si substrate.

(B) RCWA calculated total transmission into the device layer of SOI, total reflection by the SiO_2 film, and total transmission into the SiO_2 film of incident light versus period (in the x direction) for hexagonal hole array with a diameter of 700 nm on an SOI substrate. Note that the calculation is for cylindrical holes.

Table 1: Deflection angles (θ_N) of transmitted waves in the SOI device layer at different periods (p) and orders (N).

p (nm)	1000	1200	1300	1700
$\theta_{N=1}$ (°)	13.47	11.19	10.32	7.87
$\theta_{N=2}$ (°)	27.76	22.84	20.99	15.9
$\theta_{N=3}$ (°)	44.32	35.6	32.51	24.27
$\theta_{N=4}$ (°)	68.67	50.92	45.77	33.23

so we divide the transmission diffraction efficiency for each order, except $T_{N=0}$, into two equal parts with deflection angles calculated using p_x (Table 1) and p_y (not shown here), respectively.

$$\sin \theta_N = \frac{N\lambda}{pn_{\text{Si}}} \quad (6)$$

The back-reflection (R'_N) of the transmitted wave (T_N) in the SOI device layer at the Si/SiO₂ interface can be calculated based on the deflection angle (θ_N) of the transmitted wave and the critical angle of total reflection ($\theta_c = 23.79^\circ$). The formulas are shown in Section S2 in Supplementary Material. The deflection angle of the transmitted wave increases with diffraction order for a fixed period, which means that only limited orders of transmitted waves in the SOI device layer can transmit further into the SiO₂ film with a reflection of R'_N and a transmission of $1 - R'_N$. Table 1 shows that all the transmitted waves in the SOI device layer with orders $N \geq 3$ will be totally reflected. Total reflection also occurs when $N=2$ at a period of 1000 nm. The angle of reflection equals the angle of incidence at the SiO₂ film surface, which is the same as the deflection angle (θ_N) of the transmitted wave in the SOI device layer. Therefore, the back-reflected wave will be incident at the hole-based *i*-Si layer from the bottom with an angle of θ_N . The deflection angle of transmitted wave depends on the period of hole array for each diffraction order.

Based on transmission diffraction efficiencies at different orders (T_N), the total back-reflection (R'_{total}) by the SiO₂ film of incident light can be calculated using Eq. (7) and the results are shown in Figure 3B. The total transmission into the SOI device layer (T_{total}) and the SiO₂ film ($T_{\text{total}} - R'_{\text{total}}$) at different periods are also presented. As 20%–35% of the total incident light, depending on the period of the holes, will be reflected back into the *i*-Si layer that has integrated holes, the total transmission into the SiO₂ film is reduced to about 35%–45% of the incident light compared to a total transmission of about 65%–70% of the incident light into the Si substrate in the absence of the SiO₂ film. It is shown that, at a smaller period ($p=1000$ nm), ~50% of the transmitted wave in the SOI

device layer will be reflected. This is because a smaller period leads to a higher deflection angle of the transmitted wave, which results in higher reflection at the Si/SiO₂ interface.

$$R'_{\text{total}} = \sum_N T_N R'_N \quad (7)$$

The analysis shows that, except for the 0th-order ([0 0]) transmitted light, all other transmitted light with higher grating orders undergo deflections with different deflection angles after the diffraction in the hole array. The deflection of incident light affects light propagation in photodiodes from two aspects. First, laterally propagating waves are generated and increase the effective optical path in the hole-based *i*-Si layer for enhanced absorption. Calculation suggests that, for a vertically illuminated photodiode with integrated holes of diameter/period (d/p) of 700/1000 nm, 67% of the total incident light will be transmitted into the device layer of an SOI and only 12.14% of which is the 0th-order wave that does not experience deflection. This means that 54.86% of the total incident light (81.9% of the transmitted light) deflects from incidence direction and causes laterally propagating modes. Second, the higher deflection angle of the transmitted wave results in higher back-reflection at the Si/SiO₂ interface. It can be calculated that only 18% of the transmitted light in the SOI device layer will be reflected by the SiO₂ film for photodiodes without photon-trapping holes. This can be increased to 50% due to laterally propagating waves generated by the hole array and higher-order back-reflection caused by the SiO₂ film.

3.3 Absorption calculated by RCWA and measured EQE of photodiodes with integrated holes

As we have discussed previously, in our photodiodes fabricated on the SOI wafers, ~50% of the transmitted light into the SOI device layer may be reflected back by the BOX layer and interact with the *i*-Si layer for further absorption. However, the light reflected from the SiO₂ film will not be all absorbed by the *i*-Si layer as there is a transmission loss into the air-photodiode interface. Here, we also use the RCWA method to calculate the transmission diffraction efficiency (T'_N) of light incident from the bottom of the *i*-Si layer that is integrated with holes. In this calculation, the SOI device layer is used as the incident layer (assumed to have an infinite thickness), whereas air is treated as the substrate of the hole integrated *i*-Si layer. The incident

light ($T_N R'_N$), as shown in Figure 4A (inset), has an incident angle equal to the deflection angle (θ_N ; Table 1) of transmitted wave (T_N) in the SOI device layer with a diffraction order of N . For the i -Si layer with an integrated hole array with a diameter of 700 nm, transmission diffraction efficiencies of incident light from the bottom with diffraction orders from $N=0$ to $N=4$ at different periods (p) are shown in Figure 4A (period is considered in the x direction). The analysis reveals that, for each period, there are relatively high transmission diffraction efficiencies for incident light with diffraction orders $N=0$ and $N=1$, whereas the transmission are very low for higher orders. In other words, the incident light with orders $N \geq 2$ will be trapped in the photodiode structure. This is because the incident angle of light, which is equal to the deflection angle of transmitted light in the SOI device layer (θ_N), increases with the diffraction order (N). Higher incident angle means longer optical propagating path in the hole-based i -Si layer for absorption. It seems that the top surface of the i -Si layer and the bottom Si/SiO₂ interface form a kind of cavity, and most of the light with orders $N \geq 2$ will be trapped (absorbed or reflected back and forth) in the cavity until fully absorbed. Even for light with low incident angles at diffraction orders $N=0$ and $N=1$, more and more light will be trapped after being reflected and diffracted several times by hole-based i -Si layer as the incident angle keeps increasing due to the deflection of diffraction light.

Taking into account the transmission into air for incident light from the bottom with diffraction orders $N=0$ ($T'_N = 0$) and $N=1$ ($T'_N = 1$), the total transmission loss of incident light (T'_{total}) from the hole-based i -Si layer

into air can be calculated using Eq. (8), and the results are shown in Figure 4B. The total back-reflection by the SiO₂ film (R'_{total}) and increased absorption (light trapped in the hole-based i -Si layer, $R'_{\text{total}} - T'_{\text{total}}$) at different periods are also presented. It shows that only less than 5% of the total incident light will be transmitted into air after the reflection on the SiO₂ film. Most of the reflected light from the SiO₂ film will be trapped by the photodiode structure for enhanced absorption and higher EQE. The total absorption (A_{total}) of photodiodes on the SOI wafer can then be calculated using Eq. (9), taking into account the reflection from the top i -Si surface (R_{total}), transmission into the SiO₂ film ($T_{\text{total}} - R'_{\text{total}}$), and transmission loss into air of the reflected light from the SiO₂ film (T'_{total}). R_{total} and T_{total} (transmission into the device layer of SOI) in Eq. (9) for hole arrays on the SOI substrate are assumed to be the same for hole arrays on the bulk Si substrate as shown in Figures 2A and 3A, respectively.

$$T'_{\text{total}} = T_{N=0} R'_{N=0} T'_{N=0} + T_{N=1} R'_{N=1} T'_{N=1} \quad (8)$$

$$A_{\text{total}} = 1 - R_{\text{total}} - (T_{\text{total}} - R'_{\text{total}}) - T'_{\text{total}} \quad (9)$$

Figure 5A shows the RCWA calculated absorption and experimentally measured EQE of photodiodes on the SOI wafer with hole arrays in hexagonal lattice with diameters of 630 and 700 nm at different periods. The measured EQE of hole-based photodiodes fabricated on the bulk Si substrates are also presented. Generally, the experimentally measured EQE of photodiodes on an SOI wafer match well with the RCWA calculation for both diameters of 630 and 700 nm. The RCWA calculated absorption are lower

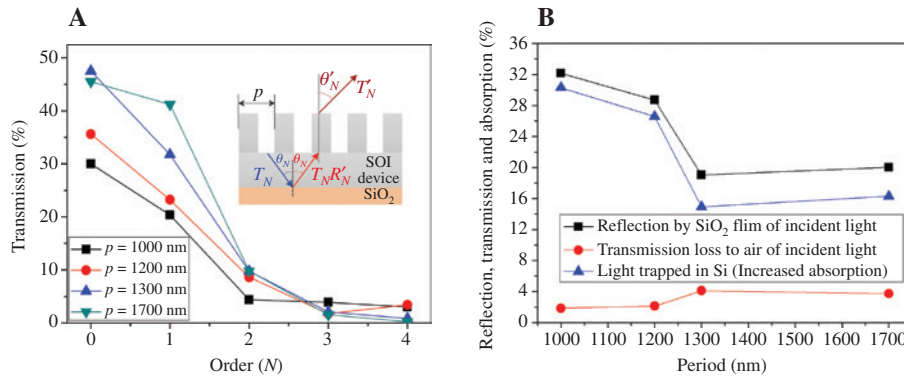


Figure 4: Calculated transmission loss and increased absorption for the light reflected by SiO₂ film.

(A) RCWA calculated transmission (T'_N) into the i -Si layers with integrated holes for incident light ($T_N R'_N$) from the bottom of the device with diffraction orders from $N=0$ to $N=4$ for varying periods (p). N is the diffraction order of transmitted light (T_N) reflected by the SiO₂ film and T'_N is the total transmission loss for the M th-order incident light. (Inset) Schematic diagram of the transmitted light (T_N) reflected by the SiO₂ film and incident to the i -Si layer from the bottom of the device ($T_N R'_N$) and then transmitted into air through the top (T'_N). (B) Calculated total reflection by the SiO₂ film, total transmission loss into air, and increased absorption of incident light at different periods (in the x direction as shown in Figure 1E). The holes are arranged in hexagonal lattice with a diameter of 700 nm on an SOI substrate.

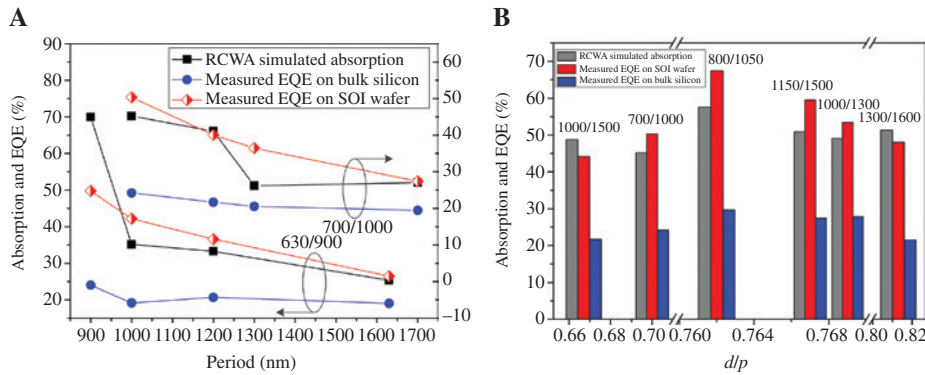


Figure 5: Calculated absorption and measured EQE of photodiodes with integrated photon-trapping holes.

(A) RCWA calculated absorption versus period for cylindrical hole arrays on the SOI wafer and experimentally measured EQE versus period for funnel-shaped hole-based photodiodes on bulk Si and SOI wafer. The holes are arranged in hexagonal lattice with diameters (d) of 630 and 700 nm. (B) RCWA calculated absorption versus d/p for cylindrical hole arrays on the SOI wafer and experimentally measured EQE versus d/p for funnel-shaped hole-based photodiodes on bulk Si and SOI wafer. The holes are arranged in hexagonal lattice with d/p in 0.65–0.85. Period (p) means the period in the x -direction.

than experimentally measured EQE for the reason that the reduced reflection of funnel-shaped holes is not counted compared to the cylindrical holes. The photodiodes with hole array with $d/p=630/900$ nm have relatively low measured EQE compared to the calculated absorption up to $\sim 74\%$. This may be caused by fabrication tolerance, reduced carrier collection efficiency caused by the narrow spacing between adjacent holes and possible presence of traps and defects in the holes that can contribute to high recombination rate. At diameters of both 630 and 700 nm, the EQE of the photodiodes on the SOI wafer are 30%–50%, whereas the photodiodes on the bulk Si substrate are only 20%–25% as the period varies.

As we have discussed before, hole arrays provide laterally propagating waves due to the deflection of light and they are trapped inside the Si layer with the help of the BOX layer of the SOI substrate due to back-reflection. In the case of bulk Si wafer, holes can generate lateral waves but as there is no back-reflection and thus high transmission to the substrate, these lateral waves are not trapped but are leaking away from the substrate. When the diameter of the holes is a constant, there is a trend that a smaller period (higher d/p) generally leads to a better EQE performance of the photodiodes. Based on our analysis, this is attributed to the more significant reduction in both reflection and transmission at a lower period, which allows more light trapped and absorbed in the i -Si layer. As higher absorption can be achieved for photodiode with hole array with higher d/p , we fabricated more photodiodes with d/p between 0.65 and 0.85, including 800/1050 nm (0.762), 1000/1300 nm (0.769), 1000/1500 nm (0.667), 1150/1500 nm (0.767), and 1300/1600 nm (0.813). The RCWA calculated absorption of hole-based i -Si layers

on the SOI wafer and the measured EQE of the photodiodes fabricated on the SOI wafer and bulk Si substrate are shown in Figure 5B. Compared to hole-based photodiodes on the bulk Si substrate with EQE of only 20%–25%, the photodiodes fabricated on the SOI wafer provide high EQE of 45%–55% with d/p in this range. This agrees well with the RCWA calculation. The highest EQE of 55% is achieved by hole-based photodiode with $d/p=800/1050$ nm.

RCWA in this work provides theoretical explanation for light trapping and absorption enhancement of photodiodes with integrated holes designed on SOI wafers. The theoretically calculated absorption of the hole-based i -Si layer shows a good agreement with the experimentally measured EQE of the photodiode. However, we have to point out that the absorption are approximately calculated values for photodiodes on the SOI wafer with multiple reflection and diffraction effects. For the sake of simplicity, some approximations are used in the calculations. (i) The incident layer (air) and substrate layer are assumed to have infinite thickness for the RCWA model used; (ii) although the impact of tapered sidewalls of funnel-shaped holes is considered in the analysis of reduced reflection, to avoid complexity in the calculations, holes are considered as cylindrical in shape in diffraction efficiency calculations; and (iii) the absorption in the SOI's device layer with a thickness of 0.25 μm is neglected when calculating the absorption of the reflected light from the BOX layer. Actually, the analysis of light propagation reveals that, in our photodiode with photon-trapping holes on the SOI wafers, light is effectively trapped between the top Si surface and the BOX layer of an SOI substrate. Light absorption takes place in both the p - i - n photodiode structure and the 0.25- μm -thick SOI device

layer. Unlike the photogenerated carriers in the *i*-Si layer, which can be quickly collected in a drift field, the minority carriers generated in the *p*, *n* and the device layer of the SOI experience a slow diffusion to the *i* region. This is a likely source of the residual photocurrent tail as reported in our earlier published work [27]. Further RCWA and high-speed measurements can be done in the future to identify where light is trapped in the multilayer photodiode and thus reduce the photocurrent tail.

Based on the design of hole array in hexagonal lattice with $d/p=700/1000$ nm, we fabricated photodiodes with different hole shapes (cylindrical and funnel) and substrates (bulk Si and SOI wafer). Flat Si PIN photodiodes with an *i*-layer thickness of 2 μm on both bulk Si and SOI substrates were also fabricated. The EQE of the photodiodes were measured at the wavelength of 850 nm. The calculated absorption of a flat Si PIN photodiode on the bulk Si substrate is 10%, and its EQE was measured to be 11.14%. Based on the calculated absorption and measured EQE of the flat device, Figure 6 shows the EQE enhancement of photodiodes with light-trapping holes on an SOI substrate. The calculated absorption or measured EQE is also shown for each device in the figure. It is shown that both the absorption and EQE of the photodiodes are enhanced by light-trapping hole structures on both bulk and SOI substrates. The measured EQE of the photodiode with a cylindrical hole array on the bulk Si substrate is 18.94%, which is a little higher than the calculation (14.17%). This can be attributed to the diffusion of photogenerated carriers generated in the thick Si wafer underneath the device.

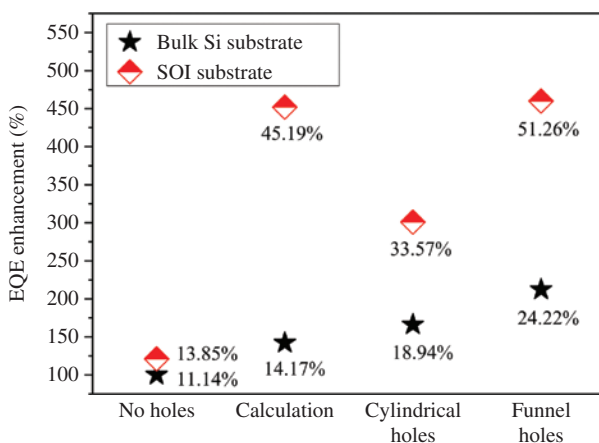


Figure 6: The EQE enhancement (relative to a device without holes on bulk Si substrates) of photodiodes with light-trapping holes on SOI substrates at the wavelength of 850 nm. The calculated absorption or measured EQE is also shown for each device. Holes are arranged in hexagonal lattice with a d/p of $d/p=700/1000$ nm. The calculation was done for cylindrical holes only.

The improvement of EQE on the SOI substrate can be observed for both flat devices and devices with integrated holes. By integrating the same cylindrical hole structures, EQE is enhanced by 166% on the bulk Si wafer and 300% on the SOI wafer, respectively. Hole arrays enable laterally propagating waves in photodiodes on both substrates. However, the EQE improvement is much more significant on the SOI substrate compared to the bulk Si substrate as more effective light trapping in the *i*-Si layer is facilitated by the presence of the BOX layer that causes back-reflection. For photodiodes on an SOI substrate, an EQE improvement of $\sim 50\%$ can be further achieved by substituting the cylindrical holes by funnel-shaped holes that contribute to lower surface reflection and results in more than 450% enhancement in a photodiode compared to the counterpart without any light-trapping holes.

4 Conclusion

In this study, microscale and nanoscale light-trapping hole arrays were integrated into photodiodes with a thin absorption region to achieve high EQE while ensuring an ultrafast response. Both theoretically and experimentally, the absorption and EQE performances of hole-based photodiodes were presented with different substrates, hole shapes, and dimensions. Our experimental results showed that, at the datacom wavelength of 850 nm, photodiodes with integrated funnel-shaped holes exhibit EQE of 20%–25% on bulk Si and 45%–55% on the SOI wafers in devices with an *i*-Si layer thickness of 2 μm . The highest EQE represents more than 500% improvement compared to similar Si photodiodes without any photon-trapping holes. The RCWA method was applied to calculate the reflection and transmission efficiencies in Si with hole arrays on both bulk and SOI substrates. The analysis showed that laterally propagating waves are generated due to the deflection of light subsequent to the diffraction in the hole array. This increases the optical propagating path in the *i*-Si layer enabling enhanced absorption. In contrast, the deflected light on the SOI substrate undergoes additional back-reflection at the Si/SiO₂ interface contributing to lower transmission loss. Funnel-shaped holes with tapered sidewalls also significantly reduce the reflection from the top surface of the photodiodes. Light is observed to remain more effectively confined in the thin Si layer on the SOI substrates rather than on the bulk Si substrates, which agrees well with our experimental results. Our all-Si photodiode, fabricated using CMOS-compatible processes, offers great potential to reduce the cost of short-reach (<300 m) communication links in data centers.

Acknowledgments: The authors thank S.P. Wang and S.Y. Wang Partnership for the financial support. Partial support from the Army Research Office (grant W911NF-14-4-0341, Funder Id: <http://dx.doi.org/10.13039/100000183>) is gratefully acknowledged.

Disclosures: The authors declare that there are no conflicts of interest related to this article.

References

- [1] Sun C, Wade MT, Lee Y, et al. Single-chip microprocessor that communicates directly using light. *Nature* 2015;528:534–8.
- [2] Tatum JA, Gazula D, Graham LA, et al. VCSEL-based interconnects for current and future data centers. *J Lightwave Technol* 2015;33:727–32.
- [3] Green MA, Keevers MJ. Optical properties of intrinsic silicon at 300 K. *Prog Photovoltaics* 1995;3:189–92.
- [4] Zhang ZM, Wang LP. Measurements and modeling of the spectral and directional radiative properties of micro/nanostructured materials. *Int J Thermophys* 2013;34:2209–42.
- [5] Homola J, Koudela I, Yee SS. Surface plasmon resonance sensors based on diffraction gratings and prism couplers: sensitivity comparison. *Sens Actuators B Chem* 1999;54:16–24.
- [6] McPhedran RC, Maystre D. A detailed theoretical study of the anomalies of a sinusoidal diffraction grating. *J Mod Optics* 1974;21:413–21.
- [7] Chen Y-B, Tan K-H. The profile optimization of periodic nanostructures for wavelength-selective thermophotovoltaic emitters. *Int J Heat Mass Tran* 2010;53:5542–51.
- [8] Maruyama S, Kashiwa T, Yugami H, Esashi M. Thermal radiation from two-dimensionally confined modes in microcavities. *Appl Phys Lett* 2001;79:1393–5.
- [9] Wang LP, Zhang ZM. Resonance transmission or absorption in deep gratings explained by magnetic polaritons. *Appl Phys Lett* 2009;95:111904.
- [10] Hu L, Chen G. Analysis of optical absorption in silicon nanowire arrays for photovoltaic applications. *Nano Lett* 2007;7:3249–52.
- [11] Garnett E, Yang P. Light trapping in silicon nanowire solar cells. *Nano Lett* 2010;10:1082–7.
- [12] Dutta AK, Olah R, Mizuno G, et al. High-efficiency solar cells based on micro-nano scale structures. *Proc SPIE* 2010;7683:768300.
- [13] Basu S, Chen Y-B, Zhang ZM. Microscale radiation in thermophotovoltaic devices – a review. *Int J Energy Res* 2007;31:689–716.
- [14] Kelzenberg MD, Boettcher SW, Petykiewicz JA, et al. Enhanced absorption and carrier collection in Si wire arrays for photovoltaic applications. *Nat Mater* 2010;9:239–44.
- [15] Zhang A, Kim H, Cheng J, Lo Y-H. Ultrahigh responsivity visible and infrared detection using silicon nanowire phototransistors. *Nano Lett* 2010;10:2117–20.
- [16] Lin H, Cheung H-Y, Xiu F, et al. Developing controllable anisotropic wet etching to achieve silicon nanorods, nanopencils and nanocones for efficient photon trapping. *J Mater Chem A* 2013;1:9942–6.
- [17] Rockstuhl C, Lederer F. Photon management by metallic nanodiscs in thin film solar cells. *Appl Phys Lett* 2009;94:213102.
- [18] Zhu J, Yu Z, Burkhard GF, Hsu C-M, et al. Optical absorption enhancement in amorphous silicon nanowire and nanocone arrays. *Nano Lett* 2008;9:279–82.
- [19] Shrestha A, Mizuno G, Oduor P, Dutta AK, Dhar NK, Lewis JS. Flexible solar cells based on curved surface nano-pyramids. *Proc SPIE* 2016;9865:986504.
- [20] Shrestha A, Mizuno G, Oduor P, Dutta AK, Dhar NK. Broadband antireflection with curved surface nano-pyramids for image sensing devices. *Proc SPIE* 2016;9854:985406.
- [21] Han SE, Chen G. Optical absorption enhancement in silicon nanohole arrays for solar photovoltaics. *Nano Lett* 2010;10:1012–5.
- [22] Morsy AM, Povinelli ML, Hennessy J. Highly selective aluminum plasmonic filters on silicon. *Opt Express* 2018;26:22650–7.
- [23] Leem JW, Joo DH, Yu JS. Biomimetic parabola-shaped AZO subwavelength grating structures for efficient antireflection of Si-based solar cells. *Sol Energy Mater Solar C* 2011;95:2221–7.
- [24] Yang L, Xuan Y, Han Y, Tan J. Investigation on the performance enhancement of silicon solar cells with an assembly grating structure. *Energy Convers Manage* 2012;54:30–7.
- [25] Hava S, Auslender M. Design and analysis of low-reflection grating microstructures for a solar energy absorber. *Solar Energy Mater Solar C* 2000;61:143–51.
- [26] Cheng Q, Li P, Lu J, Yu X, Zhou H. Silicon complex grating with different groove depths as an absorber for solar cells. *J Quant Spectrosc Radiat Transfer* 2014;132:70–9.
- [27] Gao Y, Cansizoglu H, Polat KG, et al. Photon trapping microstructures enable high-speed high efficiency silicon photodiodes. *Nat Photon* 2017;11:301–8.
- [28] Gao Y, Cansizoglu H, Ghandiparsi S, et al. A high speed surface illuminated Si photodiode using microstructured holes for absorption enhancements at 900–1000 nm wavelength. *ACS Photonics* 2017;4:2053–60.
- [29] Cansizoglu H, Bartolo-Perez C, Gao Y, et al. Surface-illuminated photon-trapping high-speed Ge-on-Si photodiodes with improved efficiency up to 1700 nm. *Photonics Res* 2018;6:734–42.
- [30] Moharam MG, Grann EB, Pommet DA. Formulation for stable and efficient implementation of the rigorous coupled-wave analysis of binary gratings. *J Opt Soc Am A* 1995;12:1068–76.
- [31] Peng S, Morris GM. Resonant scattering from two-dimensional gratings. *J Opt Soc Am A* 1996;13:993–1005.
- [32] Moharam MG, Gaylord TK. Coupled-wave analysis of two-dimensional gratings. *Proc SPIE* 1986;883:8–11.
- [33] Peng S, Morris GM. Efficient implementation of rigorous coupled-wave analysis for surface-relief gratings. *J Opt Soc Am A* 1995;12:1087–96.
- [34] Li L. New formulation of the Fourier modal method for crossed surface-relief gratings. *J Opt Soc Am A* 1997;14:2758–67.
- [35] Noponen E, Turunen J. Binary high-frequency-carrier diffractive optical elements: electromagnetic theory. *J Opt Soc Am A* 1994;11:1097–109.
- [36] Xi J-Q, Schubert MF, Kim JK, et al. Optical thin-film materials with low refractive index for broadband elimination of Fresnel reflection. *Nat Photon* 2007;1:176–9.

Supplementary Material: The online version of this article offers supplementary material (<https://doi.org/10.1515/nanoph-2019-0164>).